



# Magnetic Field Dependence of Bipolar Magnetic Region Tilts on the Sun: Indication of Tilt Quenching

Bibhuti Kumar Jha<sup>1</sup>, Bidya Binay Karak<sup>1,2</sup> , Sudip Mandal<sup>3</sup>, and Dipankar Banerjee<sup>1,4,5</sup> 

<sup>1</sup> Indian Institute of Astrophysics, Koramangala, Bangalore 560034, India; [bibhuti.kj@iiaf.res.in](mailto:bibhuti.kj@iiaf.res.in), [maitraibibhu@gmail.com](mailto:maitraibibhu@gmail.com)

<sup>2</sup> Department of Physics, Indian Institute of Technology (Banaras Hindu University), Varanasi, India; [karak.phy@iitbhu.ac.in](mailto:karak.phy@iitbhu.ac.in)

<sup>3</sup> Max-Planck-Institut für Sonnensystemforschung, Justus-von-Liebig-Weg 3, D-37077 Göttingen, Germany

<sup>4</sup> Center of Excellence in Space Sciences India, IISER Kolkata, Mohanpur 741246, West Bengal, India

<sup>5</sup> Aryabhata Research Institute of Observational Sciences, Nainital-263002, Uttarakhand, India

Received 2019 August 16; revised 2019 December 12; accepted 2019 December 28; published 2020 January 22

## Abstract

The tilt of the bipolar magnetic region (BMR) is crucial in the Babcock–Leighton process for the generation of the poloidal magnetic field in the Sun. Based on the thin flux-tube model of the BMR formation, the tilt is believed to be caused by the Coriolis force acting on the rising flux tube of the strong toroidal magnetic field from the base of the convection zone. We analyze the magnetic field dependence of BMR tilts using the magnetograms of the Michelson Doppler Imager (1996–2011) and Helioseismic and Magnetic Imager (2010–2018). We observe that the distribution of the maximum magnetic field ( $B_{\max}$ ) of BMRs is bimodal. Its first peak at the low field corresponds to BMRs that do not have sunspots as counterparts in the white-light images, whereas the second peak corresponds to sunspots as recorded in both type of images. We find that the slope of Joy’s law ( $\gamma_0$ ) initially increases slowly with the increase of  $B_{\max}$ . However, when  $B_{\max} \gtrsim 2$  kG,  $\gamma_0$  decreases. Scatter of the BMR tilt around Joy’s law systematically decreases with the increase of  $B_{\max}$ . The decrease of observed  $\gamma_0$  with  $B_{\max}$  provides a hint to a nonlinear tilt quenching in the Babcock–Leighton process. We finally discuss how our results may be used to make a connection with the thin flux-tube model.

*Unified Astronomy Thesaurus concepts:* [Bipolar sunspot groups \(156\)](#); [Solar cycle \(1487\)](#); [Solar physics \(1476\)](#); [Solar active region magnetic fields \(1975\)](#); [Solar activity \(1475\)](#); [Solar active regions \(1974\)](#)

## 1. Introduction

Sunspots are the regions of concentrated magnetic field observed as dark spots in white-light images. In the magnetograms, we find two regions of opposite polarities appearing close to each other. Thus, the sunspots that we see in white-light images are essentially two poles of a more general feature called bipolar magnetic regions (BMR). However, the weaker BMRs produce negligible intensity contrast and hence go undetected in white-light images. In general, BMRs are tilted with respect to the equator, and statistically, this tilt increases with latitude—popularly known as Joy’s law (Hale et al. 1919).

The tilt is crucial for the generation of the poloidal magnetic field through the decay and dispersal of the BMRs near the solar surface, which is popularly known as the Babcock–Leighton process. While this was proposed in the 1960s by Babcock (1961) and Leighton (1964), in recent years, this process has received significant attention due to its support from observational studies (Dasi-Espuig et al. 2010; Kitchatinov & Olemskoy 2011; Muñoz-Jaramillo et al. 2013; Priyal et al. 2014). Based on this Babcock–Leighton process, several surface flux transport models have been constructed, which are successful in reproducing many features of the magnetic field on the solar surface (Jiang et al. 2014). Many dynamo models, including the popular flux transport dynamo models, have also been constructed based on this Babcock–Leighton process (Leighton 1969; Wang & Sheeley 1991; Wang et al. 1991); see reviews by Charbonneau (2010), Karak et al. (2014), and Choudhuri (2018).

A serious concern in these Babcock–Leighton models is the saturation of magnetic field. There must be a nonlinear quenching to suppress the growth of magnetic field in any kinematic dynamo model such as the Babcock–Leighton ones. In the latter models, large-scale velocities, namely, meridional

flow and differential rotation, are specified (broadly through observations), while the small-scale velocity is parameterized such as in the form of turbulent diffusivity. Therefore, the most obvious choice in these models is to include a nonlinearity in the Babcock–Leighton process. In all the previous Babcock–Leighton dynamo models, a magnetic field dependent quenching is included such that the poloidal field production is reduced when the toroidal magnetic field exceeds the so-called saturation field  $B_0$  (Charbonneau 2010). For the Babcock–Leighton process, this requires that the tilt must be reduced when the BMR field strength exceeds a certain value; see Lemerle & Charbonneau (2017) and Karak & Miesch (2017, 2018) for specific requirements of this idea.

We believe that the BMRs are produced due to the buoyant rise of the strong toroidal magnetic flux tubes from the base of the convection zone (CZ; Parker 1955). From the thin flux-tube model, we know that during the rise of toroidal flux in the CZ, the Coriolis force induced by the diverging east–west velocity near the loop apex causes a tilt (D’Silva & Choudhuri 1993; Fan et al. 1994). Therefore, we expect the rise time of the toroidal flux tube and thus the tilt to decrease with the increase of magnetic field in the tube. This idea can potentially lead to a quenching in the Babcock–Leighton process.

Although the thin flux-tube model explains some observed features of BMRs, it does not capture the detailed dynamics of solar CZ. Indeed, including the convection, Weber et al. (2011) find a significant change in the behavior of BMR tilt. They find the tilt to increase with the magnetic field first and then decrease in accordance with the thin flux-tube model.

Using magnetogram data corresponding to 1988–2001, Tian et al. (2003) found a systematic variation of the BMR tilt with the magnetic flux content. Surprisingly, using Michelson

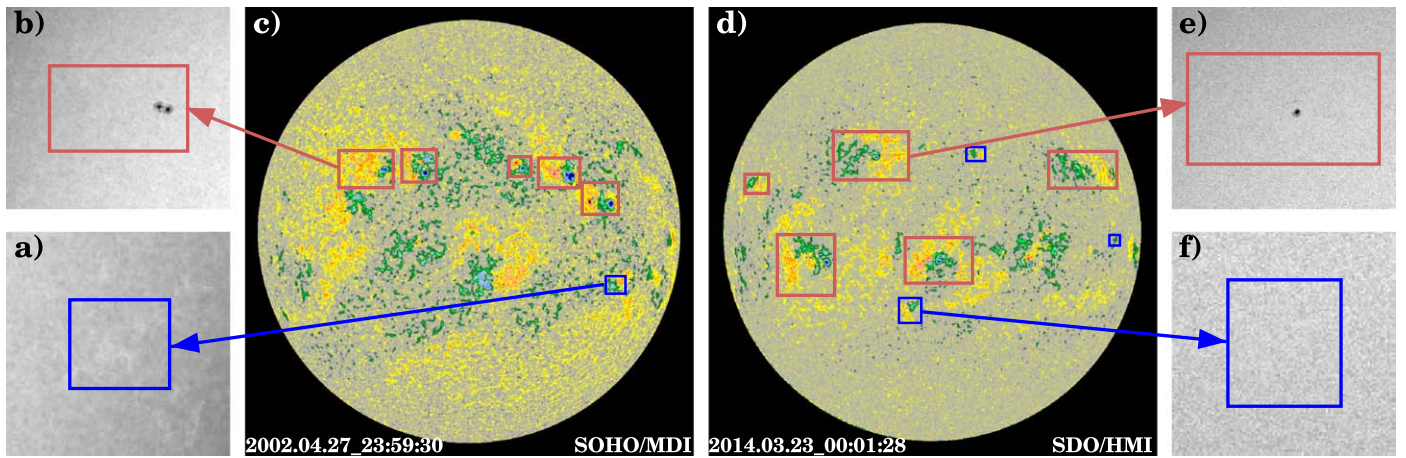


**Figure 1.** Representative magnetograms of (c) MDI and (d) HMI (saturated to  $\pm 1.5$  kG) with BMR<sub>WS</sub> (red box) and BMR<sub>NS</sub> (blue). Panels (a), (b), (e), and (f) show IC counterparts.

Doppler Imager (MDI) magnetograms during 1996–2011, Stenflo & Kosovichev (2012) did not find any systematic variation of the BMR tilt with the magnetic flux, and they claim that their result rules out the thin flux-tube model. However, we should not forget that the magnetic fields of BMRs also vary with the magnetic flux (Tlatov & Pevtsov 2014), and in the analysis of Stenflo & Kosovichev (2012), the variation of magnetic field is ignored. Therefore, the motivation of the present Letter is first to analyze the BMRs based on their magnetic field strength. Then we shall check how the tilt changes with the magnetic field strength and whether there is any quenching in the tilt to support the theoretical models of BMR formation and the Babcock–Leighton dynamo saturation.

## 2. Data and Method

In this work, we have used the full disk line-of-sight (LOS) magnetogram with a cadence of 6 hr and intensity continuum (IC) with a cadence of 24 hr from MDI (1996–2011; Scherrer et al. 1995) and the Helioseismic and Magnetic Imager (HMI: 2010–2018; Schou et al. 2012) for identification of BMRs.

The magnetograms taken from these two instruments give only the LOS component of the magnetic field. To get the magnetic field in the direction normal to the solar surface we have corrected for the projection effect. The projection effect becomes more and more critical as we go toward the limb of the solar disk. Therefore, in the first step, we have restricted ourselves up to  $0.9R_{\odot}$ . Later on, to avoid the uncertainty in the magnetic field measurement we have also excluded the BMRs that have absolute mean heliographic longitude greater than  $50^{\circ}$  from our analysis.

To identify BMRs, we have followed the method given in Stenflo & Kosovichev (2012). So we have first applied a threshold on magnetic field strength and then a moderate flux balance condition to avoid the false detection of a unipolar spot or BMR with a large flux difference (see Figures 1(c)–(d)). Unlike Stenflo & Kosovichev (2012), we have applied a 2D Gaussian smoothing with an FWHM of 3 pixels (Hagenaar et al. 1999) to reduce the spatial noise, before calculating (I) heliographic coordinate, (II) magnetic flux, and (III) maximum field density from detected BMRs. Since the maximum magnetic field density mimics the maximum field strength, we call it the maximum field strength  $B_{\max}$ . While calculating  $B_{\max}$  for HMI data, we have multiplied it by a factor of 1.4 to bring two data

sets on the same scale (Liu et al. 2012). Tilts of BMRs have been calculated with respect to the solar E–W direction considering the spherical geometry of the Sun.

## 3. Results and Discussions

Before we explore the magnetic field dependence of the BMR tilt, we first present the distribution of the maximum magnetic field  $B_{\max}$  of BMRs in Figures 2(a)–(b). For the time being, we ignore the solid and dashed lines in these figures. We observe two well-separated peaks at around 600 and 2100 G. These peaks are seen both in MDI and HMI data. HMI data include solar cycle 24, which is a relatively weak cycle and contains fewer strong-field BMRs compared to weak-field BMRs. Despite the data obtained from two different instruments and two different solar cycles, we find the presence of two distinct peaks in both data sets. These two distinct peaks remain even when we do not smooth the data or smooth with different windows. However, as we smooth the data with a wider averaging window, these peaks tend to flatten out as well as shift slightly toward lower values. In the extreme limit, when we take the average magnetic field (i.e., window size equal to the BMR area), the two observed peaks disappear. This is expected because the magnetic field falls rapidly as we move away from the BMR center.

It appears that the whole HMI distribution is slightly shifted to the left side and therefore the peaks appear at slightly smaller  $B_{\max}$  than in the MDI data. This could be due to different solar cycles, or it could be that the factor 1.4 used to scale the HMI magnetic field is not appropriate for the entire range of  $B_{\max}$  (Liu et al. 2012; Pietarila et al. 2013). Nevertheless, these results suggest that the magnetic field distribution of BMRs is bimodal and possibly there are two types of BMRs having significantly different field strengths.

To understand these two peaks in our data, we analyze their IC for the same periods. The IC images may not necessarily be simultaneous but they are near-simultaneous with a maximum time difference of 3 hr. We find that not all BMRs have their counterparts in IC (i.e., sunspots; Figures 1(a) and (f)). When we say counterpart in IC, we mean whether there is any spot present in the IC on the BMR region (as identified in the magnetogram), independent of their size. It turns out that the BMRs that have their counterparts in IC (Figures 1(b) and (f)) have a higher magnetic field. When we overplot these two

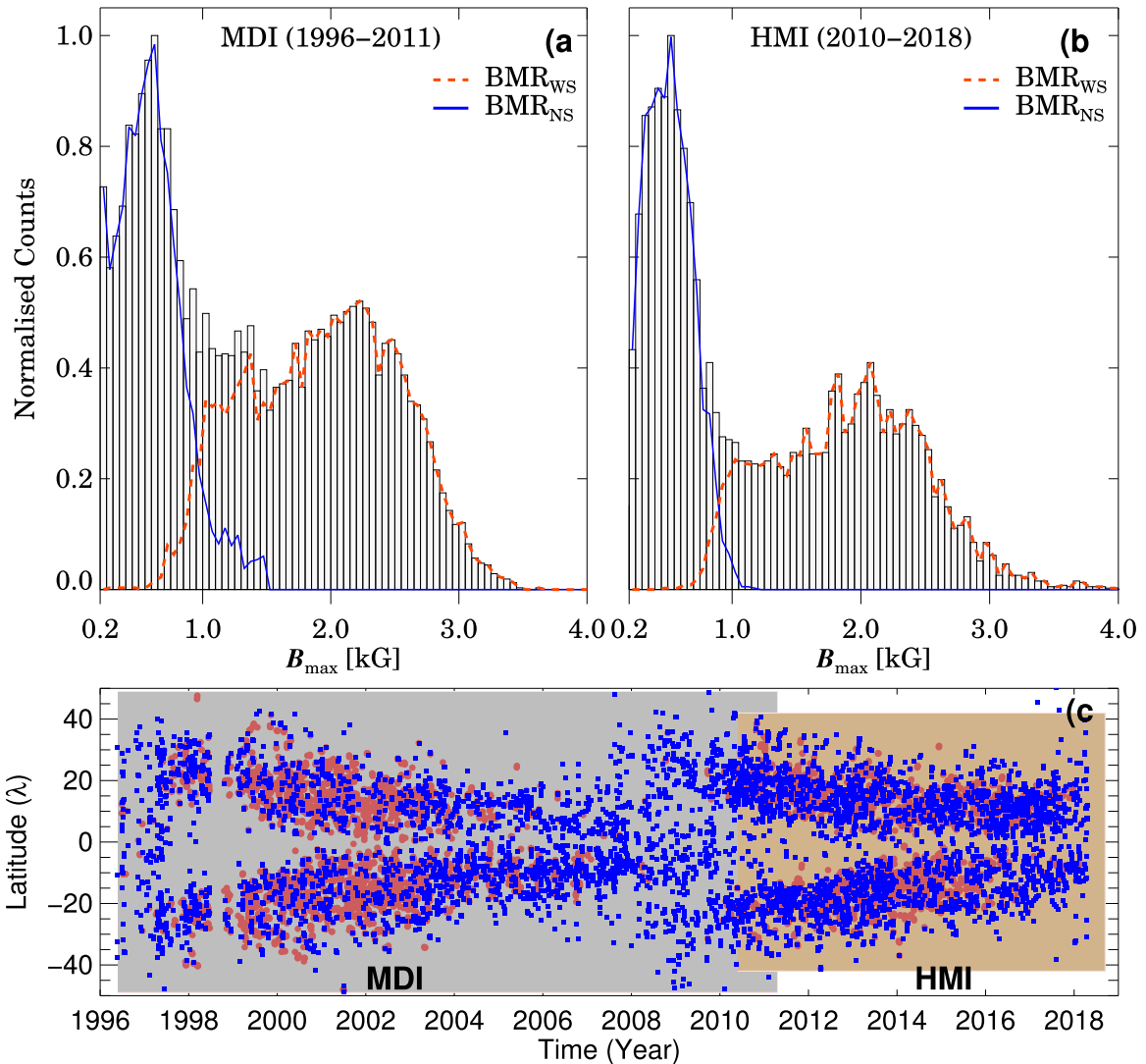


**Figure 2.** (a)–(b) Distributions of  $B_{\max}$  in the BMRs from MDI (left panel) and HMI (right). Red and blue, respectively, show  $B_{\max}$  distributions of  $BMR_{WS}$  (having a counterpart in IC) and  $BMR_{NS}$  (no counterpart in IC). The vertical axes of the two panes are divided by 315 and 388, respectively, to bring the maxima of distributions to unity. (c) Time–latitude distribution of  $BMR_{WS}$  (red) and  $BMR_{NS}$  (blue).

distributions in Figure 2, we find that the BMRs with counterparts in IC (red/dashed line) beautifully represent the second peak at high  $B_{\max}$  and the rest, i.e., BMRs without a counterpart in IC (blue line), overlap with the first peak at low  $B_{\max}$ . Again, we notice that in both the data sets this feature distinctly appears. We define  $BMR_{WS}$  as the BMRs that have a counterpart in IC, i.e., no sunspots and  $B_{\max}$  distribution peaks at around 2 kG, while  $BMR_{NS}$  is defined as the BMRs that do not have sunspots (no counterpart in IC) and  $B_{\max}$  distribution peaks at around 600 G. Similar bimodality in the maximum field distribution has been reported in the past by Cho et al. (2015) and Tlatov et al. (2019) using sunspots and pores from SDO/HMI data. However, in our work we look into the more general features, BMRs, of which sunspots and pores are a part.

Seeing the peak of  $BMR_{NS}$  at a smaller field strength, one may conjecture that these BMRs are produced from the small-scale magnetic field possibly originating from the small-scale dynamo (Petrovay & Szakaly 1993). If this is the case, then we expect no preferred latitude distribution and no solar cycle variation. However, in Figure 2(c), we find no such evidence. Both classes of BMRs follow similar temporal and latitudinal

variations in the usual butterfly diagram. Thus, this result does not suggest that the origins of  $BMR_{NS}$  are linked to the small-scale dynamo.

Now we explore the magnetic field dependence of BMR tilt. As we have found two distributions of BMRs, we shall first present the basic features of the tilt of these two BMR classes separately. Figure 3 shows the tilt distributions of these two classes of BMRs, namely,  $BMR_{WS}$  (red) and  $BMR_{NS}$  (blue), in the latitude range  $10^{\circ}$ – $30^{\circ}$  including both hemispheres. Distributions peak at nonzero tilt and show Gaussian-like behavior, which is of course not new (Wang & Sheeley 1989; Stenflo & Kosovichev 2012). Although both distributions peak almost at the same tilt value, the distribution spreads are not identical and they are consistently different in the two data sets. After fitting histograms with Gaussian profiles with mean  $\mu$  and standard deviation  $\sigma$ , we find  $\mu$  is around  $9^{\circ}$  for both classes of BMRs and from both data sets. However,  $\sigma$  for  $BMR_{WS}$  is smaller by a few degrees in both the data sets. These results indicate that the tilt has some magnetic field dependence.

As shown in Figures 3(c)–(d), Joy’s law slope  $\gamma_0$  is consistently different in the two classes of BMRs.  $BMR_{WS}$

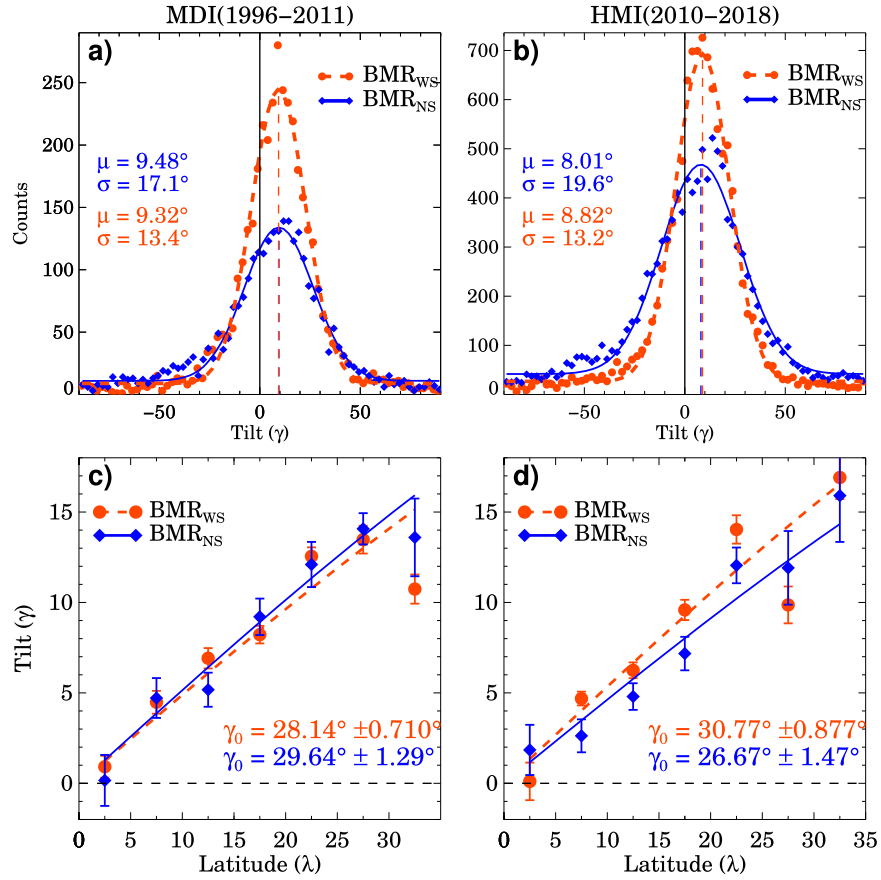


**Figure 3.** (a)–(b) Red and blue show tilt distributions of BMR<sub>WS</sub> and BMR<sub>NS</sub>, respectively. Points represent the data, and lines show the fitted Gaussians with parameters marked on the panels. (c)–(d) Mean tilt in each latitude bin as a function of the latitude. Solid and dashed lines are Joy’s law ( $\gamma = \gamma_0 \sin \lambda$ ) fits for BMR<sub>WS</sub> and BMR<sub>NS</sub>.

has a slightly larger  $\gamma_0$  in HMI data, while in MDI data it is the opposite. As MDI and HMI include data from two different times, we do not expect the Joy’s law trend to be identical in the two data sets. Nonetheless, evidence of Joy’s law in BMR<sub>NS</sub> further suggests that the BMR<sub>NS</sub> class may not be originating from the small-scale magnetic field, rather they must be originating from the same large-scale magnetic field that produces BMR<sub>WS</sub>.

### 3.1. Magnetic Quenching of Tilt Angle

To quantify the magnetic field dependence of the BMR tilt, we now compute Joy’s law slope  $\gamma_0$  and the scatter around the mean tilt ( $\sigma$ ), separately in each  $B_{\max}$  bin with a bin size of 500 G. In Figure 4(a), we observe that for MDI data  $\gamma_0$  is only slightly increased in the small  $B_{\max}$  range and then dropped at least by about 15° in the high-field values above 2 kG. While HMI data follow a general trend, there is a significant increase in the low-field range. A prominent reduction of  $\gamma_0$  (by about 15°) with the magnetic field strength clearly establishes the existence of BMR tilt quenching. We emphasize that the tilt quenching is seen when  $B_{\max} > 2$  kG. That is why in Figure 3 the mean Joy’s law trend of BMR<sub>WS</sub> is not smaller than BMR<sub>NS</sub>. It is only the strong BMR<sub>WS</sub> having  $B_{\max} > 2$  kG that show the quenching in tilt.

We note that although the general trend of tilt quenching is seen, the results are slightly sensitive to the analysis, particularly to the number of data. We have checked that our results do not change drastically when (i) taking different  $B_{\max}$

bins, (ii) excluding data points if Joy’s law fit is not significant, and (iii) removing the data in the Joy’s law fitting if the BMR number is less than 50 in each latitude bin. Further, the different behavior of MDI and HMI always persists. As seen in Figure 4(b), the variation with the BMR flux is monotonous for MDI data but not for HMI.

The indication of tilt quenching as seen in Figure 4(a) gives an observation support of the following nonlinear quenching in the Babcock–Leighton  $\alpha$  or in  $\gamma_0$  routinely used to saturate the magnetic field growth in kinematic dynamo models (e.g., Choudhuri et al. 1995; Dikpati & Charbonneau 1999; Chatterjee et al. 2004; Karak et al. 2019):

$$f_q \propto \frac{1}{\left[1 + \left(\frac{B_{\max}}{B_0}\right)^n\right]} \quad (1)$$

with  $n = 2$  (see, for example, Equation (10) of Karak & Miesch 2017). However, our data fits best when  $n = 5.8 \pm 0.8$  (and  $B_0 = 2.9 \pm 0.1$  kG with reduced- $\chi^2 = 30.9$ ).

Now we discuss whether our results can be connected to the theory of the thin flux-tube model for the BMR formation. Based on this theory, we expect the intense toroidal flux rises fast, and thus the Coriolis force gets less time to induce a tilt. Hence, the BMR tilt is expected to decrease with the increase of the magnetic field. The thin flux-tube simulations of Fan et al. (1994) predicted

$$\gamma \propto \sin \lambda B_0^{-5/4} \Phi^{1/4}, \quad (2)$$

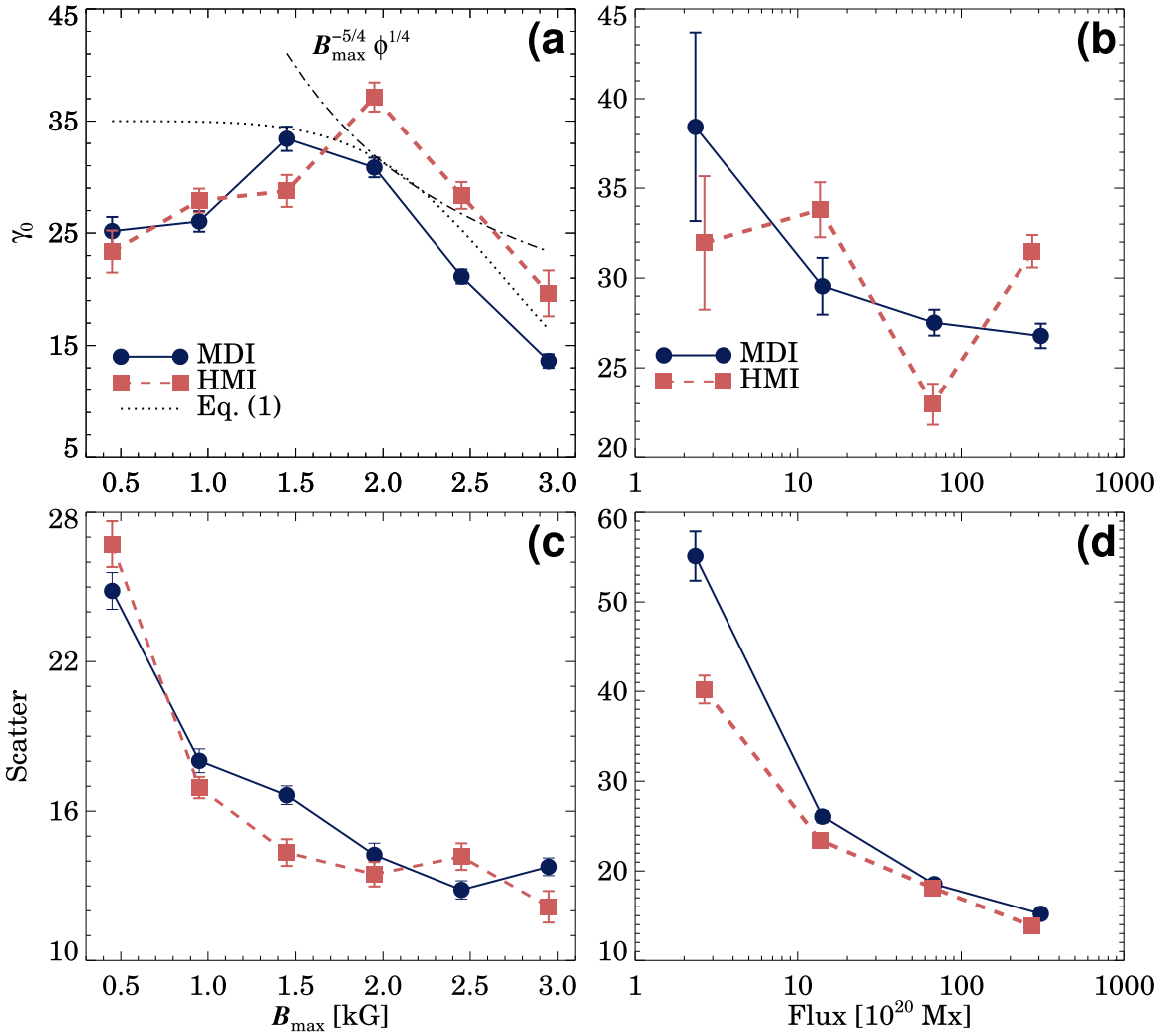


**Figure 4.** Magnetic field ( $B_{\max}$ ) dependences of (a) Joy’s law slope  $\gamma_0$  and (c) the tilt scatter  $\sigma$ . Panels (b) and (d) are the same as the left panels but as functions of flux.

where  $B_0$  is the initial magnetic field of the toroidal flux tube and  $\Phi$  is the flux content. The theoretical study suggests that due to the combined effects of rapid expansion, radiative cooling, and pressure buildup, the magnetic fields of BMRs forming loops become sufficiently low as they rise toward the surface, and within a few Mm depth BMRs tends to get disconnected from their roots (Schüssler & Rempel 2005). The current understanding of the whole process is very limited; however, see Rempel & Cheung (2014), Fan & Fang (2014), Nelson et al. (2014), and Işık (2015). Therefore, we do not know whether the initial magnetic field  $B_0$  is related to the  $B_{\max}$  that we observe inside the BMR. However, if we assume that  $B_0 \propto B_{\max}$ , then we can make some comment on the thin flux-tube model.

The BMR flux  $\Phi$  is observed to vary with the magnetic field strength (Tlatov & Pevtsov 2014). In our data, we find the following relation holds reasonably well:

$$\frac{\Phi}{\langle \Phi \rangle} = a + b \frac{B_{\max}}{\langle B_{\max} \rangle} + c \left( \frac{B_{\max}}{\langle B_{\max} \rangle} \right)^2 + d \left( \frac{B_{\max}}{\langle B_{\max} \rangle} \right)^3, \quad (3)$$

where  $a = -0.08 \pm 0.01$ ,  $b = 0.84 \pm 0.12$ ,  $c = -0.57 \pm 0.19$ , and  $d = 0.52 \pm 0.08$  for MDI data and  $a = -0.09 \pm 0.02$ ,

$b = 0.81 \pm 0.15$ ,  $c = -0.27 \pm 0.23$ , and  $d = 0.32 \pm 0.10$  for HMI. Putting this relation in Equation (2), we find that the slope of Joy’s law  $\gamma_0$  decreases as shown by the dashed line. We observe that in the high-field regime, our result qualitatively supports the thin flux-tube model.

In the low-field regime with  $B_{\max} < 2$  kG  $\gamma_0$  increases with  $B_{\max}$ , which does not fit with the thin flux-tube model. However, we should not forget that this model does not include the convection, which can affect the dynamics of the flux tube to change the tilt through the helical convection. By considering convection, in the thin flux-tube model, Weber et al. (2011) showed that while the general Joy’s law trend is recovered, the tilt increases with the increase of magnetic field strength first in the low-field regime, and then it reduces; see their Figures 8 and 12 (also see Weber et al. 2013). Similar behavior is found in our data; see Figure 4(a).

Thin flux-tube rise model also predicted that the rising flux loops could be buffeted by the turbulent convection during their rise in the CZ and this could cause a scatter around the systematic tilt variations—Joy’s law (Longcope & Fisher 1996; Longcope & Choudhuri 2002). When the magnetic field is strong, we expect the magnetic tension to oppose this buffeting of flux tubes and the scatter to be less. Further, strong flux tubes rise faster (due to strong magnetic buoyancy) and thus they get

less time to be buffeted by convection (Weber et al. 2011). The tilt scatter computed from our data supports this idea. In Figures 4(c)–(d), we see that it systematically decreases with the increase of  $B_{\max}$  or flux.

#### 4. Conclusion

In this Letter, we have studied BMRs detected from the magnetograms of MDI (1996–2011) and HMI (2010–2018). In both the data sets, we find that the BMR number distribution shows a bimodal distribution when measured with respect to their maximum magnetic field  $B_{\max}$ . The first peak at low field ( $B_{\max} \approx 600$  G) corresponds to BMRs that do not have counterparts in IC (i.e., no sunspots), while the second peak at high field ( $B_{\max} \approx 2100$  G) corresponds to BMRs that have counterparts in IC.  $BMR_{NS}$  also shows a similar butterfly diagram, tilt distribution, and Joy’s law as that of  $BMR_{WS}$ . This suggests that  $BMR_{NS}$  class is not produced from the small-scale magnetic field, rather it must be produced from the same large-scale global field that produces sunspots. One difference between these two classes of BMRs is that the tilt scatter and the slope of Joy’s law  $\gamma_0$  are different. However, our study does not explain why BMRs show two distinct peaks in the  $B_{\max}$  distribution, which requires further studies.

On computing the tilt in each  $B_{\max}$  bin, we find a significant change in the BMR tilt for MDI and HMI data. In the low  $B_{\max}$  range,  $\gamma_0$  increases with the increase of  $B_{\max}$ . However, for  $B_{\max} > 2$  kG (which corresponds to strong sunspots),  $\gamma_0$  decreases with  $B_{\max}$ . These results are in qualitative agreement with the predictions of the thin flux-tube rise model (D’Silva & Choudhuri 1993; Fan et al. 1994; Caligari et al. 1995; Fan 2009) and in particular the simulations with the convection (Weber et al. 2011, 2013). The reduction of tilt with the increase of the magnetic field in the high-field regime gives a hint for the nonlinear quenching routinely used in the Babcock–Leighton-type kinematic dynamo models.

We understand that the variations of BMR properties, particularly the tilt quenching with the magnetic field, are demonstrated in a relatively narrow range. This, however, is due to the fact that the availability of data is limited and Joy’s law is a statistical relation. Furthermore, the last two cycles, during which our analyses are performed, are relatively weak, having weak BMR field strength. The highest magnetic field in our BMRs data is about 3 kG, and the magnetic quenching is expected to be more in the super-kilogauss magnetic field. Therefore, we believe that our results need to be investigated further with larger data sets, especially from stronger cycles having high-field BMRs.

We thank the anonymous referee for the detailed comments that helped to clarify some issues in the revised manuscript. B.B. K. sincerely acknowledges financial support from Department of Science and Technology (SERB/DST), India through the Ramanujan Fellowship (project No. SB/S2/RJN-017/2018).

He further appreciates loving hospitality at Indian Institute of Astrophysics, Bangalore during this project.

#### ORCID iDs

Bidya Binay Karak  <https://orcid.org/0000-0002-8883-3562>  
Dipankar Banerjee  <https://orcid.org/0000-0003-4653-6823>

#### References

- Babcock, H. W. 1961, *ApJ*, **133**, 572  
 Caligari, P., Moreno-Inertis, F., & Schussler, M. 1995, *ApJ*, **441**, 886  
 Charbonneau, P. 2010, *LRSP*, **7**, 3  
 Chatterjee, P., Nandy, D., & Choudhuri, A. R. 2004, *A&A*, **427**, 1019  
 Cho, I.-H., Cho, K.-S., Bong, S.-C., et al. 2015, *ApJ*, **811**, 49  
 Choudhuri, A. R. 2018, *JASTP*, **176**, 5  
 Choudhuri, A. R., Schüssler, M., & Dikpati, M. 1995, *A&A*, **303**, L29  
 Dasi-Espuig, M., Solanki, S. K., Krivova, N. A., Cameron, R., & Peñuela, T. 2010, *A&A*, **518**, A7  
 Dikpati, M., & Charbonneau, P. 1999, *ApJ*, **518**, 508  
 D’Silva, S., & Choudhuri, A. R. 1993, *A&A*, **272**, 621  
 Fan, Y. 2009, *LRSP*, **6**, 4  
 Fan, Y., & Fang, F. 2014, *ApJ*, **789**, 35  
 Fan, Y., Fisher, G. H., & McClymont, A. N. 1994, *ApJ*, **436**, 907  
 Hagenaar, H. J., Schrijver, C. J., Title, A. M., & Shine, R. A. 1999, *ApJ*, **511**, 932  
 Hale, G. E., Ellerman, F., Nicholson, S. B., & Joy, A. H. 1919, *ApJ*, **49**, 153  
 Işık, E. 2015, *ApJL*, **813**, L13  
 Jiang, J., Hathaway, D. H., Cameron, R. H., et al. 2014, *SSRv*, **186**, 491  
 Karak, B. B., Jiang, J., Miesch, M. S., Charbonneau, P., & Choudhuri, A. R. 2014, *SSRv*, **186**, 561  
 Karak, B. B., & Miesch, M. 2017, *ApJ*, **847**, 69  
 Karak, B. B., & Miesch, M. 2018, *ApJL*, **860**, L26  
 Karak, B. B., Tomar, A., & Vashishth, V. 2019, *MNRAS*, **2813**  
 Kitchatinov, L. L., & Olemskoy, S. V. 2011, *AstL*, **37**, 656  
 Leighton, R. B. 1964, *ApJ*, **140**, 1547  
 Leighton, R. B. 1969, *ApJ*, **156**, 1  
 Lemerle, A., & Charbonneau, P. 2017, *ApJ*, **834**, 133  
 Liu, Y., Hoeksema, J. T., Scherrer, P. H., Schou, J., & Couvidat, S. 2012, *SoPh*, **279**, 295  
 Longcope, D., & Choudhuri, A. R. 2002, *SoPh*, **205**, 63  
 Longcope, D. W., & Fisher, G. H. 1996, *ApJ*, **458**, 380  
 Muñoz-Jaramillo, A., Dasi-Espuig, M., Balmaceda, L. A., & DeLuca, E. E. 2013, *ApJL*, **767**, L25  
 Nelson, N. J., Brown, B. P., Brun, A. S., Miesch, M. S., & Toomre, J. 2014, *SoPh*, **289**, 441  
 Parker, E. N. 1955, *ApJ*, **121**, 491  
 Petrovay, K., & Szakaly, G. 1993, *A&A*, **274**, 543  
 Pietarila, A., Bertello, L., Harvey, J. W., & Pevtsov, A. A. 2013, *SoPh*, **282**, 91  
 Priyal, M., Banerjee, D., Karak, B. B., et al. 2014, *ApJL*, **793**, L4  
 Rempel, M., & Cheung, M. C. M. 2014, *ApJ*, **785**, 90  
 Scherrer, P. H., et al. 1995, *SoPh*, **162**, 129  
 Schou, J., et al. 2012, *SoPh*, **275**, 229  
 Schüssler, M., & Rempel, M. 2005, *A&A*, **441**, 337  
 Stenflo, J. O., & Kosovichev, A. G. 2012, *ApJ*, **745**, 129  
 Tian, L., Liu, Y., & Wang, H. 2003, *SoPh*, **215**, 281  
 Tlatov, A., Riekhainen, A., & Tlatova, K. 2019, *SoPh*, **294**, 45  
 Tlatov, A. G., & Pevtsov, A. A. 2014, *SoPh*, **289**, 1143  
 Wang, Y. M., & Sheeley, N. R. J. 1991, *ApJ*, **375**, 761  
 Wang, Y.-M., & Sheeley, N. R., Jr. 1989, *SoPh*, **124**, 81  
 Wang, Y.-M., Sheeley, N. R., Jr., & Nash, A. G. 1991, *ApJ*, **383**, 431  
 Weber, M. A., Fan, Y., & Miesch, M. S. 2011, *ApJ*, **741**, 11  
 Weber, M. A., Fan, Y., & Miesch, M. S. 2013, *SoPh*, **287**, 239